PROCEEDINGS, 48th Workshop on Geothermal Reservoir Engineering
Stanford University, Stanford, California, February 6-8, 2023
SGP-TR-224

Harnessing the Waste Heat from Radioactive Waste in a Notional UK Geological Disposal Facility Using a Closed-Loop Geothermal System

Muhammad U. Tahir[1], Hannah R. Doran[1,2], Gioia Falcone[1], David C.W. Sanderson[2]

[1]James Watt School of Engineering, University of Glasgow, Glasgow, UK

[2] Scottish Universities Environmental Research Centre, East Kilbride, UK

Malicck14@gmail.com, h.doran.1@research.gla.ac.uk, gioia.falcone@glasgow.ac.uk, david.sanderson@glasgow.ac.uk

Keywords: closed-loop geothermal system, geological disposal facility, lower strength sedimentary rock

ABSTRACT

A permanent solution for the long-term disposal of high heat producing radioactive wastes is yet to be demonstrated. Previous research into geological disposal facilities has focused on long-term safety of a mined repository or deep borehole disposal. Due to the decay heat released from high heat producing waste, there are safety concerns, such as rock uplift, canister degradation, and potential radionuclide leakage into the surrounding rock. This paper focuses on mitigating these concerns by recovering decay heat from the rock through an 'Eavor-like' U-tube closed-loop geothermal system, with the recovered thermal energy representing a source of clean heat. The UK is seeking a mined repository in lower strength sedimentary rock, such as the Mercia Mudstone Group, and a closed-loop geothermal system is considered appropriate for such a low permeability, conductive geological setting. This paper presents an in-depth sensitivity analysis performed using a numerical/semi-analytical approach using the T2Well-EOS1/TOUGH2 software on a closed-loop geothermal system within a notional geological disposal facility using the Mercia Mudstone as the host rock. Thermal analyses were performed with different host formations and varying mass flow rate, geometry radii and lateral length for a total simulation time of 1 year. The best-case scenario identified the Tarporley Siltstone as the host rock with a 2 kg/s mass flow rate, a larger lateral radius compared to the injection/production legs (Case 3), and a lateral length of 2 km. A long-term sustainability study of 10 years was undertaken on the best-case scenario for mass flow rates of 2 kg/s and 20 kg/s, revealing that the 2 kg/s rate offered a higher outlet temperature of 19.91 °C (versus 8.06 °C) but a lower net energy flow rate of 125.80 kW (versus 258.38 kW). This study helps identify optimal CLGS design parameters within the natural LSSR environment. Future work will entail the addition of anthropogenic heat and how removing excess heat from the rock could reduce peak temperatures to improve safety concerns and the carbon footprint of current geological disposal developments.

1. INTRODUCTION

The long-term disposal of radioactive waste requires careful planning and strict safety requirements, which can delay the operational phase of a geological disposal facility (GDF). One of these safety features is to emplace high heat producing waste (HHPW) in a multi-barrier system to provide sufficient shielding and long-term integrity to the canister and surrounding rock. Decay heat released from the waste will increase the temperature of the surrounding rock formations with time, which could activate thermal-hydro-mechanical-chemical (THMC) processes in the waste and the barriers that surround it [1–3]. Therefore, removing this 'excess' heat is an important factor to improve the overall safety of the GDF. In addition, the temperature gradient surrounding the heat source term and the extent of thermal spread into the rock with time will be highly dependent on the thermal properties of the host rock. This paper focuses on a lower strength sedimentary rock setting (LSSR), as there is potential to remove this 'excess' decay heat from a low thermally conductive host rock, to reduce the peak temperatures observed near the multi-barrier system [4]. The concept of heat recovery from a GDF setting was first initiated by Chandrasekharem et al [5], where electricity production was proposed by adopting a binary cycle technology such as an Enhanced Geothermal System (EGS). However, an EGS open-loop system would increase uncertainties in canister integrity, especially if the design stimulated fracture networks near the repository. Instead, this paper proposes a closed-loop geothermal system (CLGS); in particular, an 'Eavor-like' U-tube CLGS, where pure water is pumped through the system and heated by indirect conductive heat transfer only.

A sensitivity analysis of a 1 km 'Eavor-like' U-tube CLGS is presented within an LSSR environment to represent a future GDF site to dispose of the UK's HHPW inventory. This prototype was modelled in T2Well-EOS1/TOUGH2 which was previously validated against the OpenGeoSys software, and a code developed in MATLAB by Doran et al [6]. While the heat source term from the HHPW canisters was not modelled in this sensitivity analysis, a preliminary assessment of the benchmark design is needed within the LSSR environment to assess the outlet temperatures prior to waste disposal, and how these temperatures are affected in future work with the addition of an anthropogenic heat source. The design was altered to assess the best-case scenario from altering mass flow rate of the working fluid, the wellbore radii, and lateral length, in addition to a detailed host rock assessment on the LSSR environment. Finally, a long-term sustainability comparison was made against a low (2 kg/s) versus high (20 kg/s) fixed mass flow rate. Outlet temperatures and net energy flow rates were compared against to assess this preliminary design within a future UK GDF, and future work will entail further analyses with the addition of the anthropogenic heat source term.

An overview on the UK's waste inventory is given in Section 2.1, followed by GDF and CLGS supporting literature in Sections 2.2 and 2.3 respectively. The methodology for the software, 'Eavor-like' U-tube CLGS prototype and sensitivity analysis is provided in Sections 3.1, 3.2 and 3.3 respectively. The results from the sensitivity analysis are provided in Section 4.

2. BACKGROUND THEORY

2.1 UK Radioactive Waste Inventory

Radioactive waste is a harmful by-product generated predominantly from nuclear power production and additional fuel-cycle processes [7, p.3]. Based on radioactivity levels and heat produced per unit volume, the UK categorizes this waste into distinct classes i.e. high level waste (HLW), intermediate level waste (ILW), low level waste (LLW) and very low level waste (VLLW) [8, p.14-17]. Spent nuclear fuel (SNF) tends to be separated from radioactive waste depending on a country's fuel cycle; open-loop countries (Finland and USA) include SNF, while closed-loop countries (France and UK) separate SNF from radioactive waste [7, p.27]. Nevertheless, not all the UK's SNF has undergone reprocessing activities and one should consider this alongside radioactive waste when devising a long-term disposal solution for the UK's inventory. Therefore, another term is adopted for waste needing future disposal in the UK, called high-heat producing waste (HHPW), which includes SNF (legacy waste, new build and mixed-oxide fuels), HLW, highly enriched uranium and plutonium stockpiles [9, 10, p.6]. According to a recent RWM 2021 inventory report [10, pp. 55-65], approximately 11,800 m^3 out of a total 342,000 m^3 stored waste volume is needed for disposal of HHPW from the UK's inventory, which equates to roughly 19,000 canisters requiring emplacement into the future GDF – see section 2.2.

2.2 GDF literature relevant to UK case study

The UK's HHPW inventory defined in section 2.1 should be disposed of permanently in a GDF, which is considered technologically challenging as adequate shielding is required to maintain long-term protection against radiation release from radioactive decay into the surrounding environment. The vertical depth of the GDF ranges between 0.2 – 1 km for a mined repository concept (MR), and over 1 km for a deep geological disposal concept, as previously defined by Doran et al [6]. This paper focuses on the former MR concept where waste is emplaced in tunnels that form an arrangement of panels in the subsurface. This is because the MR concept is considered the standard disposal route for most countries; examples include the Swedish KBS-3V concept [12, 13] and the Swiss Nagra concept [3, 10], where waste is encased in a multi-barrier system of manmade (waste form, canister, buffer/backfill) and natural (host rock) barriers to avert possible radiation release into the environment [9]. In particular, the UK plans to adopt the KBS-3V concept, where all HHPW is disposed of in copper canisters, surrounded by compacted bentonite buffer and backfill plug layers [9, 10, pp 55-65]. **Figure 1** illustrates the Swedish KBS-3V GDF concept, with dimensions on four panel configurations interpreted from [14].

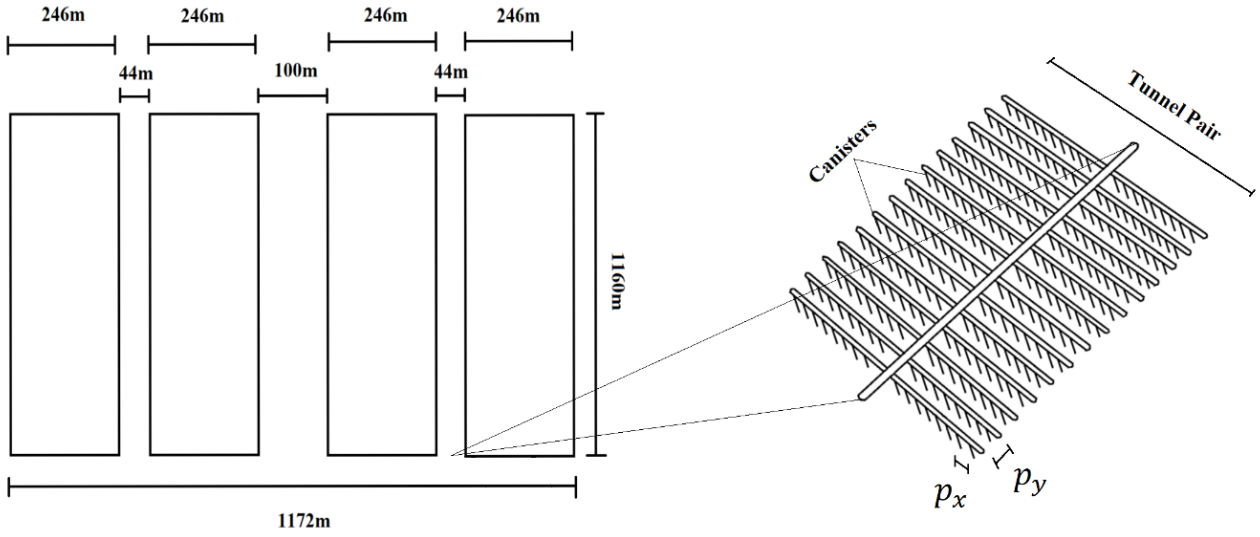

Figure 1: Schematic of part of a Swedish KBS-3V GDF panel configuration, adapted from [14].

It is important to quantify the type of geology that will host the future GDF program. A recent screening of the UK's geology selected Allerdale, Copeland, and Theddlethorpe as districts for site characterization – see **Figure 2** where colours crimson, red and black depict the regions of interest for each district respectively. All three sites at the proposed GDF vertical depth MR range consist of three host rock types: evaporite (EV), higher strength (HSR) and lower strength sedimentary (LSSR), where their recommended bulk thermal properties can be found in Jackson et al [15, p.13]. The LSSR, in particular the Mercia Mudstone group, has gained interest as a host rock candidate for chosen areas within the Allerdale and Copeland districts, but is also present onshore in the west of the Theddlehorpe district [16]. The LSSR host rock yields the smallest thermal diffusivity (lowest thermal conductivity) according to Jackson et al [15, p.13], implying that the thermal spread will be slower over time compared to the other host rocks, which could cause higher temperatures near the source term. Due to these reasons, the Mercia Mudstone group (LSSR) rock environment was chosen for further investigation and why the 'Eavor-like' U-tube CLGS design is preferred here before the addition of the anthropogenic heat source term – see Section 2.3 for details on the CLGS concept.

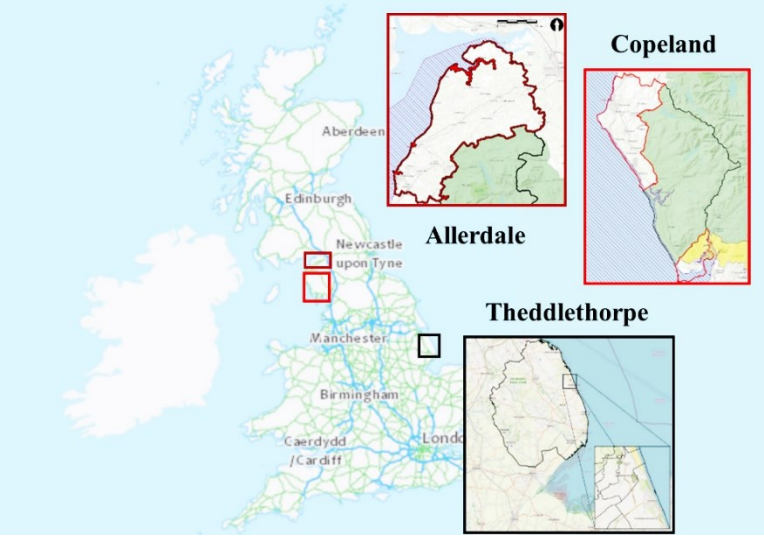

Figure 2: Map of the three UK sites for the future GDF program: Allerdale [17], Copeland [18] and Theddlethorpe [19].

2.3 CLGS literature relevant to UK case study

A GDF setting could be a favourable environment for a CLGS, since CLGS' work best in low permeability rock which is a key requirement to characterise the GDF host rock types in Section 2.2 [20, 21]. In addition, it is regarded as an enhanced closed-loop geothermal system, where the working fluid does not come into direct contact with the groundwater and is independent of reservoir properties [22, 23]. Ensuring this indirect contact between the fluid and the rock is essential to mitigate fracture networks that could provide pathways for possible radionuclide groundwater leakage after long-term waste emplacement.

Figure 3 depicts the combination of the 'Eavor-like' U-tube CLGS concept within the LSSR GDF setting (see **Figure 1**):

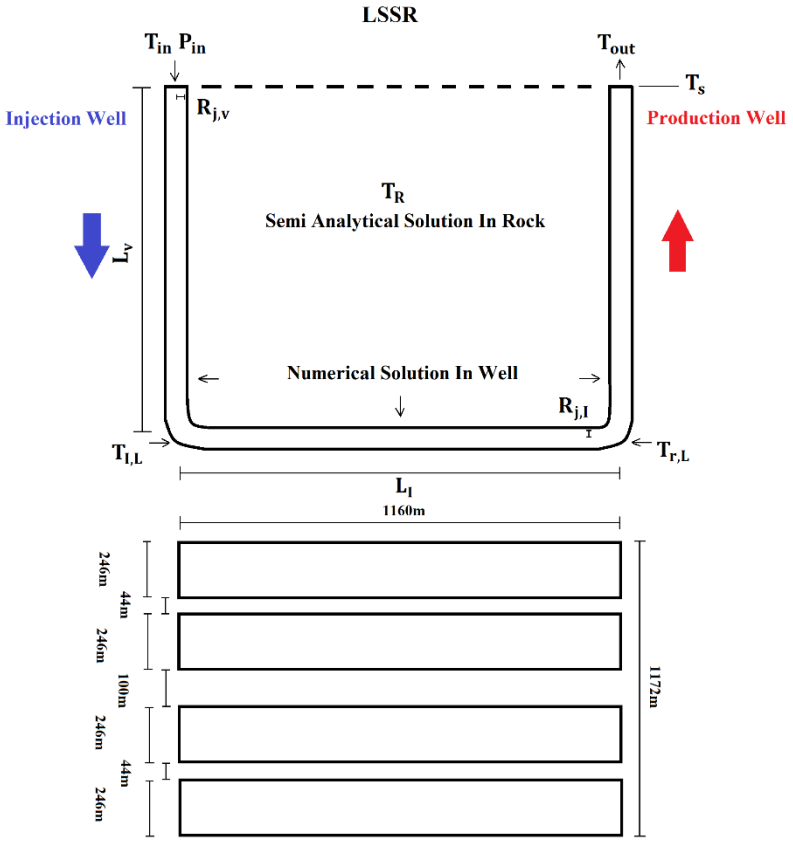

Figure 3: 'Eavor-like' U-tube CLGS concept within the LSSR GDF, adapted from [6, 14].

In general, a CLGS can be classified into two sub-categories i.e. coaxial borehole (vertical, horizontal and inclined) and U-tube heat exchangers (single or multi-lateral U-tubes) [23–27]. The latter is explored within this paper, namely a single lateral U-tube design which can be adjusted to suit the dimensions of a GDF repository highlighted in Section 2.2. Within the literature, there have been multiple studies on single lateral U-tube designs for working fluids such as CO_2 and pure water [28–32]. One study by Yuan et al [30] was adopted as an original case study for this paper; a 3 km x 4 km single lateral U-tube CLGS where water was the working fluid at constant flow rate of 5.47 kg/s. To compliment the GDF vertical depth range highlighted in Section 2.2, this case study was modified by Doran et al [6] to a 1 km x 4 km single lateral design which forms the benchmark case study for this paper (see Section 3.2). It was also identified by Tahir [33] that the lateral region of interest for extracting heat from a future GDF is between 1 km to 2 km. Therefore, further modifications were made to the benchmark case study to investigate how heat extraction at the outlet is affected by altering the lateral length to 1 km, 1.5 km, and 2 km (See Section 3.3).

3. METHODOLOGY

3.1 T2Well-EOS1/TOUGH2 software implementation

The software utilised within this paper is a numerical/semi-analytical coupled research code suited to multi-phase non-isothermal flow conditions [34]. The T2Well domain (wellbore) is discretized and solved numerically [35], while the TOUGH2 domain (reservoir) is simplified to a semi-analytical solution to reduce computational demand and with conductive rock conditions only for the CLGS [36,37]. The Equation of State (EOS1) has been utilised to represent pure water conditions under single phase flow within the wellbore [36, p.30].

Equations (1) – (5) show the conservation equations that are solved within T2Well-EOS1, where the energy accumulation M^E (2), the semi-analytical heat exchange Q_i^3 (3) and energy flux F^E (4) equations are incorporated into the total partial derivative form (1). The variables are ρ_L liquid density (kg/m^3), S_L local saturation of liquid phase, U_L internal energy of liquid phase, u_L liquid velocity of fluid (m/s), g gravitational acceleration (m/s^2), z elevation in well (m), θ inclination angle of wellbore (°), A_{wi} wellbore to formation lateral area (m^2), K_{wi} thermal conductivity of wellbore/formation (W/mK), T_i temperature in ith wellbore node (°C), T_∞ ambient temperature (°C), r radium of wellbore (m), $f(t)$ Ramey's well heat loss function, k area averaged thermal conductivity of wellbore (W/mK), σ cross sectional area of wellbore (m^2), h_L specific enthalpy of liquid phase (kJ/kg), γ slip between two phases, P pressure (Pa), Γ surface area of well side (m^2) and μ apparent friction coefficient [35].

$$\frac{\partial M^K}{\partial t} = q^K + F^K \tag{1}$$

$$M^E = \rho_L S_L \left(U_L + \frac{u_L^2}{2} + gz\cos\theta \right) \tag{2}$$

$$Q_i^3 = -A_{wi}(K_{wi}) \left[\frac{T_i - T_\infty(z)}{r f(t)} \right] + \sum_\beta (\rho_L u_L \, g \cos\theta)_i \tag{3}$$

$$F^E = -k\frac{\partial T}{\partial z} - \frac{1}{\sigma}\frac{\partial}{\partial z}\left[\sigma \rho_L S_L u_L \left(h_L + \frac{u_L^2}{2} + gz\cos\theta \right) \right] \tag{4}$$

$$\frac{\partial}{\partial t}(\rho_L u_L) + \frac{1}{\sigma}\frac{\partial}{\partial z}[\sigma(\rho_L u_L^2 + \gamma)] = -\frac{\partial P}{\partial z} - \frac{\Gamma \mu \rho_L |u_L| u_L}{2\sigma} - \rho_L g\cos\theta \tag{5}$$

As previously defined in Doran et al [6], T2Well has been applied to a deep borehole heat exchanger [38, 39], and a single lateral U-tube CLGS with a similar numerical/semi-analytical hybrid approach [29].

3.2 'Eavor-like' U-Tube benchmark case study

A benchmark case study from Doran et al [6] for a single lateral at 1 km vertical depth, 4 km lateral length, with pure water as the working fluid at the constant mass flow rate of $\dot{m} = 5.47$ kg/s, was used as a base case scenario for the sensitivity analysis. The wellbore geometry and mass flow rate were obtained from a recent Yuan et al [30] study, while the bulk thermal rock properties for the LSSR environment were taken from Jackson et al [15, p.13]. An inlet temperature of 5 °C and inlet pressure of 0.1 MPa was assumed with a geothermal gradient of 0.026 °C/m to represent UK settings [39]. **Table 1** depicts the benchmark case study for this CLGS U-tube, including rock properties, wellbore geometry, and fluid conditions:

Table 1: 'Eavor-like' U-tube CLGS benchmark case.

Lower Strength Sedimentary Rock Properties	**Value**
Thermal conductivity, k (W/mK)	1.9
Specific heat Capacity, c_P (J/kgK)	1400
Density, ρ (kg/m^3)	2100
Closed-Loop Geothermal System Geometry	
Vertical depth, L_v (m)	1000
Inner radius, $R_{j,v}$ (m)	0.105
Lateral length, L_l (m)	4000
Inner radius, $R_{j,l}$ (m)	0.078
Wellbore Fluid Conditions	
Mass flow rate, $\dot{m}$ (kg/s)	5.47
Initial Conditions	
Inlet temperature at surface, T_{in} °C	5
Inlet wellbore pressure at surface, P_{in} (MPa)	0.1
Initial temperature at 1 km °C	31
Initial pressure at 1 km (MPa)	9.9

Figure 4 illustrates the 'Eavor-like' U-tube CLGS prototype that was applied within this study, highlighting the relevant parameters from **Table 1** and where the numerical/semi-analytical parts of the code were implemented:

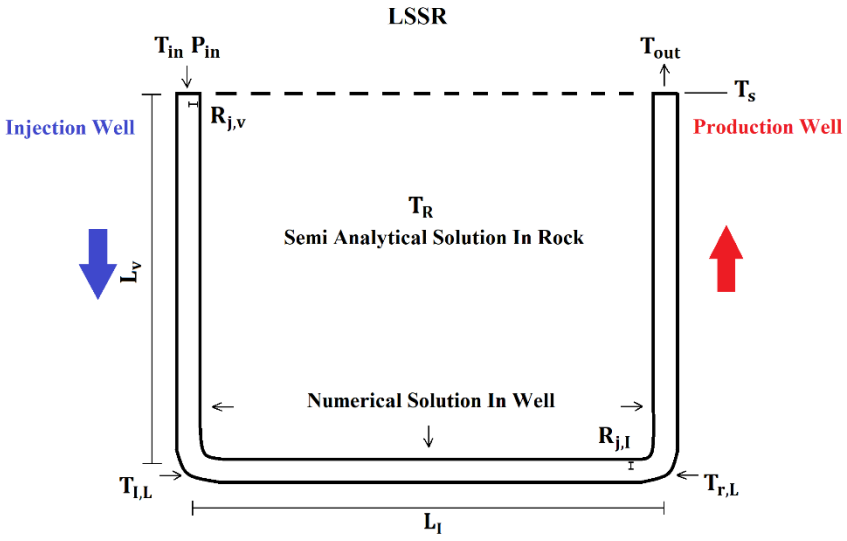

Figure 4: Schematic of a CLGS U-Tube, exemplifying the flow of the working fluid.

3.3 Sensitivity Analysis Setup

From the benchmark previously defined in Section 3.2, a sensitivity analysis on the prototype was investigated to determine the best-case scenario on the optimal outlet temperature and net energy flow rate for sufficient heat recovery purposes. Parameters such as mass flow rate (2 – 8 kg/s), host rock thermal properties, geometry radii and lateral lengths (1km, 1.5km and 2 km) was explored and the best-case

scenario in optimal outlet temperature and net energy flow rate was assumed and carried forward. Mass flow rates were picked to lie either side of the benchmark case study of 5.47 kg/s. Host rock thermal properties of the Mercia Mudstone Group were extracted from Parkes et al [41] where an average value was taken for density, specific heat capacity and thermal conductivity. The geometry radii of 0.21 m (injection/production) and 0.105 m (lateral) were previously extracted from the Yuan et al [30] study, but these parameters were swapped over to see how increasing/decreasing the lateral and injection/production sections of the CLGS could affect the temperature and net energy flow rate seen at the outlet point. Finally, lateral lengths of 1 km, 1.5 km and 2 km were chosen based on the previous GDF and CLGS lateral studies obtained from the literature in Section 2.3.

Table 2 depicts the scenarios for the sensitivity analysis in detail.

Table 2: Sensitivity analysis scenarios.

Parameters	Values	Description
$\dot{m}$	2-2.5-3-3.5-4-5-8	Mass flow rate (kg/s)
Host Lower Strength Sedimentary Rocks:		
- Arden Sandstone	1.655 2229 1051	Thermal conductivity (W/mK) Density (kg/m^3) Specific heat capacity by mass (J/Kkg)
- Sidmouth Mudstone	2.678 2454 925	Thermal conductivity (W/mK) Density (kg/m^3) Specific heat capacity by mass (J/Kkg)
- Tarporley Siltstone	2.817 2576 807	Thermal conductivity (W/mK) Density (kg/m^3) Specific heat capacity by mass (J/Kkg)
Radii:		
- Case 1	0.21 0.105	Injection/Production Well (m) Horizontal Well (m)
- Case 2	0.105	Throughout whole U-tube (m)
- Case 3	0.105 0.21	Injection/Production Well (m) Horizontal Well (m)
Lateral Lengths:	1 1.5 2	(km) (km) (km)

All scenarios were simulated for a total time of 1 year. A final comparison was made for a 10-year simulation against the best-case scenario of a low (2 kg/s) versus high (20 kg/s) mass flow rate example, to determine how these two cases performed in the GDF environment for a longer time period. The results for the long-term sustainability study are presented in Section 4.5.

4. ANALYSIS AND DISCUSSIONS

The following sections delve into the sensitivity analysis of the 'Eavor-like' U-tube CLGS benchmark design. Working fluid temperature versus vertical depth profiles and a comparison in outlet temperature and net energy flow rate values were produced for Sections 4.1 – 4.4, for a total simulation time of 1 year. Section 4.5 depicts a working fluid temperature versus time profile for the long-term sustainability analyses of the design after the best-case scenario was predicted from the previous parameter changes. In addition, a comparison of the outlet temperature and net energy flow rates were also tabulated, for a total simulation time of 10 years.

4.1 Mass Flow Rate Study

Figure 5 depicts the working fluid temperature versus the vertical depth profile for varying mass flow rates applied to the benchmark 'Eavor-like' U-tube CLGS:

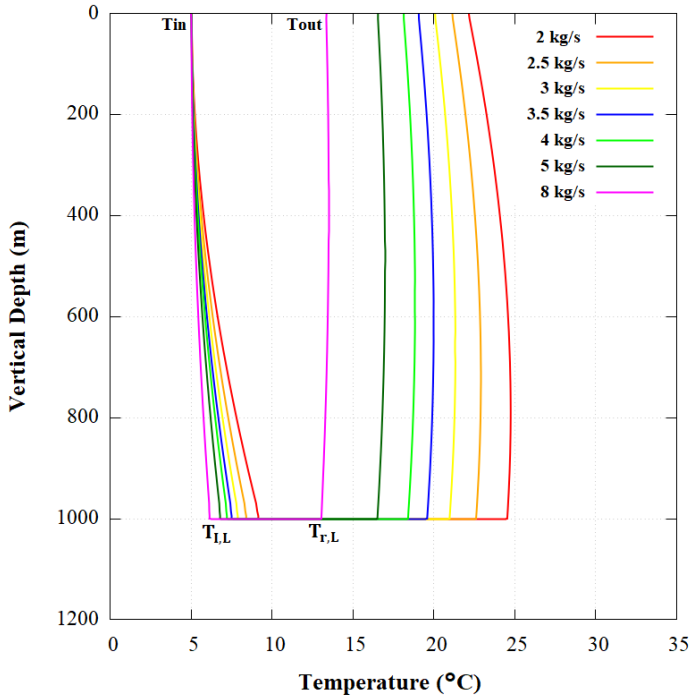

Figure 5: Working fluid temperature versus vertical depth for various mass flow rates over a simulated period of one year.

Table 3 tabulates the key outlet temperatures seen for each mass flow rate, in addition to an energy flow rate comparison against the code and theory:

Table 3: The outlet temperatures and net energy flow rates for various mass flow rates during a one-year simulation time.

Mass flow rate $\dot{m}$ (kg/s)	Outlet temperature T_{out}	$\lvert T_i - T_o \rvert$ (°C)	Q (kW) - Code
2	22.15	17.16	144.29
2.5	21.13	16.14	169.55
3	20.07	15.08	189.97
3.5	19.05	14.06	206.71
4	18.13	13.14	220.63
5	16.53	11.54	242.39
8	13.35	8.36	280.92

Referring to **Figure 5** and **Table 3**, the outlet temperature is seen to decrease from 22.15 °C to 13.35 °C when the mass flow rate has increased from 2 kg/s to 8 kg/s. This occurs because as the mass flow rate increases the residence time will decrease, and hence the working fluid is flowing at a faster rate to pick up sufficient heat transfer, especially into the lateral section. This is also backed up in the literature from Doran et al [38] when adjusting the mass flow rate within a DBHE design. However, the net energy flow rate generated is seen to increase from 144.29 kW to 280.92 kW when the mass flow rate is increased from 2 kg/s to 8 kg/s. According to Ghavidel et al [42], electricity production (and hence net energy flow rate) for an Organic Rankine Cycle on CLGS's is improved when mass flow rate increases – however, a lower flow rate would reduce the energy circulation requirement. Therefore, 2 kg/s was chosen to be the best-case scenario since it resulted in the highest outlet temperature of 22.15 °C which is desirable to improve system efficiency and could be applicable to heat recovery options such as greenhouse crop growth or 5th generation district heating network systems [44,45]. Future work on how the temperature of the rock profile changes with respect to mass flow rate is needed to quantify safety improvements to the LSSR GDF environment with the addition of the anthropogenic heat source.

4.2 Host Rock Study

Figure 6 depicts the working fluid temperature versus vertical depth profile for distinct host rock cases applied to the benchmark 'Eavor-like' U-tube CLGS along with the best-case scenario from section 4.1.

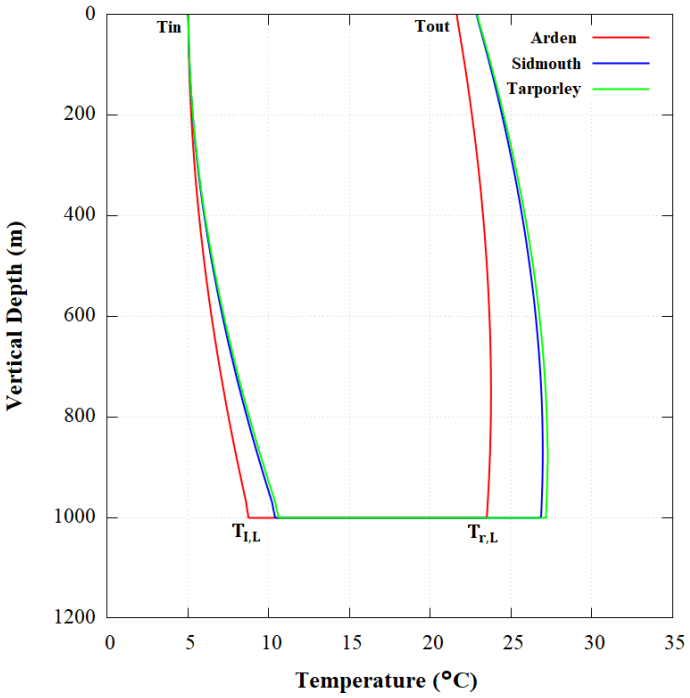

Figure 6: Working fluid temperature versus vertical depth for several host rocks in the Mercia mudstone group over a simulated period of one year.

Table 4 tabulates the key outlet temperatures seen for each host rock case, in addition to the net energy flow rate seen from the code.

Table 4: The table represents outlet temperatures and energy flow rates for distinct host rocks for 1 year simulation time.

Host Rocks	Outlet temperature T_{out}	$\lvert T_i - T_o \rvert$ (°C)	Q (kW) - Code
Arden Sandstone	21.64	16.65	139.93
Sidmouth Mudstone	22.87	17.88	150.48
Tarporley Siltstone	22.90	17.91	150.77

Referring to **Figure 6** and **Table 4**, the outlet temperature tends to increase from 21.64 °C to 22.90 °C when the host rock is changed from the Arden Sandstone to the Tarporley Siltstone. This occurs due to enhanced thermal conductivity resulting in a higher thermal diffusivity and a higher rate of heat transfer between the working fluid and the conductive rock setting, which is supported from the literature in Yuan et al [30]. Similarly, the net energy flow rate is also observed to increase from 139.93 kW to 150.77 kW along with the increase in outlet temperatures and thermal conductivity values. In summary, the Tarporley Siltstone formation is considered to be the best-case scenario from the host rock analysis because it produced the highest outlet temperature of 22.90 °C along with the highest net energy flow rate in comparison with other formations from the Mercia Mudstone Group.

4.3 Geometry radii Study

Figure 7 portrays the working fluid temperature versus vertical depth profiles for distinct geometry radii cases applied to the benchmark 'Eavor-like' U-tube CLGS along with best-case scenarios from sections 4.1 and 4.2.

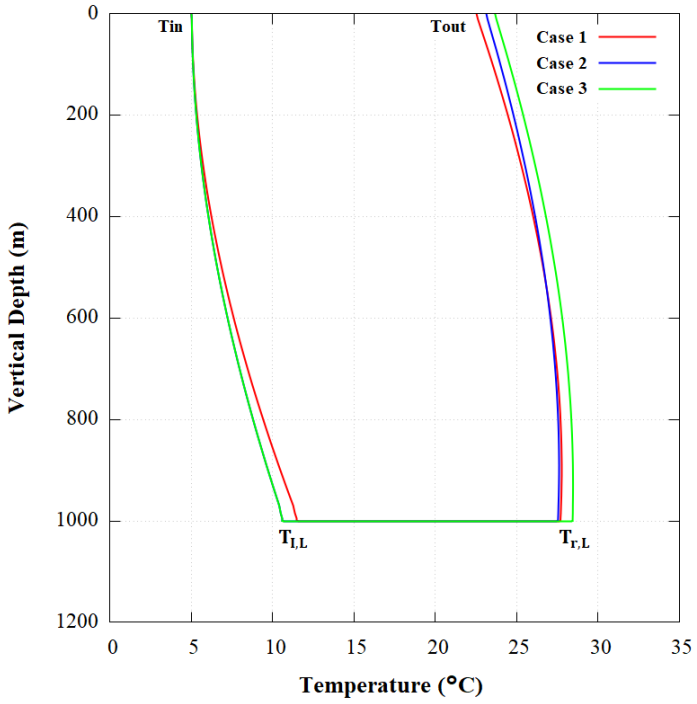

Figure 7: Working fluid temperature versus depth for different geometry radii (All Cases) over a simulated period of one year.

Table 5 tabulates the key outlet temperatures seen for each geometry radii case, in addition to the net energy flow rate from the code.

Table 5: The table represents outlet temperatures and energy flow rates for geometry radii cases for 1 year simulation time.

Case	Outlet temperature T_{out}	$\lvert T_i - T_o \rvert$ (°C)	Q (kW) - Code
1	22.52	17.53	147.68
2	23.12	18.13	152.67
3	23.66	18.67	157.20

Referring to **Figure 7** and **Table 5**, the outlet temperature is seen to increase from 22.52 °C to 23.66 °C when a larger geometry radius was given to the lateral section of the CLGS U-Tube within Case 3. This is backed up by the literature from Esmaeilpour et al [43], according to which the velocity of working fluid is proportional to the friction loss and increasing the well diameter can reduce the frictional losses. Similarly, as from **Table 5**, it can be observed that Case 3 resulted in the highest net energy flow value when the lateral diameter was a factor of two higher than the injection/production legs, but only revealing a slight increase of 10 kW when comparing against the benchmark (Case 1). This can also be supported from literature by Esmaeilpour et al [43], which states that the alteration of wellbore dimeter doesn't have significant effect on the generated power. To summarize the geometry radii study, Case 3 resulted as the best–case scenario and enhancing lateral section diameter proved to be a dominant factor while achieving a high outlet temperature and net energy flow value. However, one could argue that from a drilling perspective Case 1 could offer the cheapest option as adjusting the wellbore diameter of the lateral does not significantly affect the net energy flow rate at the outlet point.

4.4 Lateral Length Study

Figure 8 illustrates the profile for distinct lateral length cases applied to the benchmark 'Eavor-like' U-tube CLGS along with best-case scenarios from sections 4.1 – 4.3.

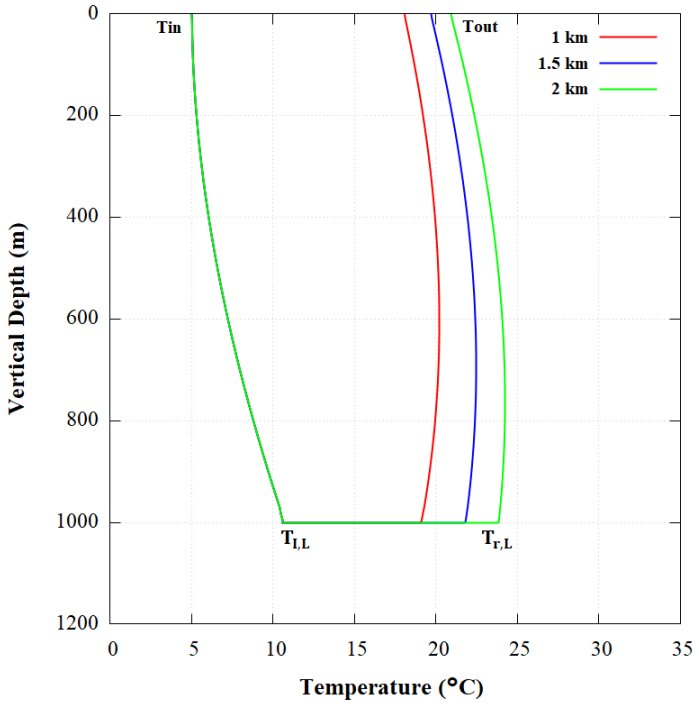

Figure 8: Working fluid temperature versus depth for different lateral lengths (All Cases) over a simulated period of one year.

Table 6 tabulates the key outlet temperatures seen for each lateral length case, in addition to the net energy flow rate seen from the code.

Table 6: The table represents outlet temperatures and energy flow rates for lateral length cases for 1 year simulation time.

Case (km)	Outlet temperature T_{out}	$\lvert T_i - T_o \rvert$ (°C)	Q (kW) - Code
1	18.07	13.08	110.19
1.5	19.69	14.70	124.90
2	20.91	15.92	134.12

Referring to **Figure 7** and **Table 6**, the outlet temperature is seen to increase from 18.07 °C to 20.91 °C when the lateral length is increased from 1 km to 2 km. This occurs because a larger lateral length increases the heat transfer area and the working fluid covers a larger distance for the heat exchange process. This is supported by literature from Song et al [28] when an increase in the length of horizontal section increases the net energy flow rate and outlet temperature. Therefore, 2 km was chosen as the best-case scenario as it offers an increase in outlet temperature (2.5 °C) and net energy flow rate (20 kW) compared with the 1 km case.

4.5 Long term sustainability

Figure 9 portrays the final comparison for a 10-year simulation against the best-case scenario of a low (2 kg/s) versus high (20 kg/s) mass flow rate example along with the best-case scenarios from sections 4.2 – 4.4, to determine how these two cases performed in the GDF environment for a longer time period.

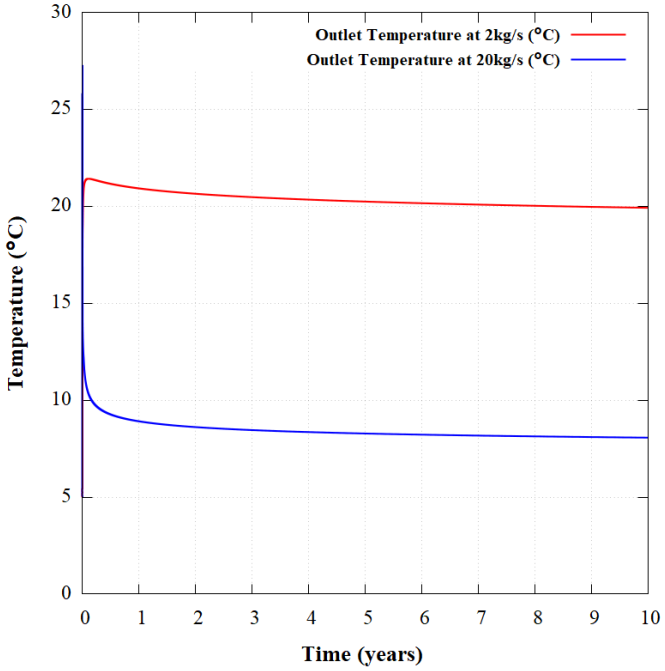

Figure 9: Working fluid temperature versus time for 2 kg/s and 20 kg/s at outlet cell throughout a 10-year simulation period.

Table 7 tabulates the key outlet temperatures seen for each flow rate case, in addition to the net energy flow rate obtained from the code.

Table 7: The table represents outlet temperatures and energy flow rates for 2kg/s and 20kg/s for 10 year simulation time.

Case (kg/s)	Outlet temperature T_{out}	$\lvert T_i - T_o \rvert$ (°C)	Q (kW) - Code
2	19.90	14.92	125.80
20	8.06	3.07	258.38

Referring to **Figure 9** and **Table 7**, the outlet temperature decreases from 19.90 °C to 8.06 °C when the mass flow rate has increased from 2 kg/s to 20 kg/s. In both cases, the outlet temperature remained constant throughout the majority of the simulation time showing that the system achieved steady state conditions after approximately 200 days. However, the net energy flow value increased from 125.80 kW to 258.38 kW when the mass flow rate increased from 2 kg/s to 20 kg/s, as previously supported by the mass flow rate study in Section 4.1. The case with 2kg/s mass flow rate resulted as the best-case scenario while achieving a high outlet temperature, however net energy flow value tends to be lower compared with 20kg/s mass flow rate case.

5. CONCLUSIONS

An 'Eavor-like' U-tube CLGS benchmark case study underwent a sensitivity analysis, where several parameters were altered to investigate the system's overall heat transfer to prepare it for a future MR GDF setting for the UK's HHPW inventory. In general, the outlet temperatures ranged from 20 °C to 26 °C, with net energy flow rates between 110 kW and 281 kW over a simulated period of one year. The mass flow rate study revealed that the 2.0 kg/s flow rate yielded the highest outlet temperature of 22.15 °C, where residence time has increased to allow a greater extent of heat transfer from the surrounding formation into the CLGS. The host rock study revealed that the Tarporley Siltstone formation from the Mercia Mudstone group proved to be most efficient resulting in the highest outlet temperature of 22.90 °C and net energy flow rate 150.77 kW. The geometry study also revealed that increasing the lateral radii compared to the injection/production legs (Case 3) produced a higher outlet temperature of 23.66 °C and higher net energy flow rate of 157.20 kW, due to lower temperature losses. However, care must be taken, and it should be well synchronized with the mass flow rate to avoid losses. Adjusting the lateral length range from 1 km to 2 km to compliment GDF settings revealed that the longer length had the highest outlet temperature of 20.91 °C and higher new energy flow rate of 134.12 kW. The findings demonstrated that the system's efficiency increased with the length of the lateral section because greater surface area was in contact with the environment during the heat transfer process. Finally, the long-term sustainability study revealed that both the 2 kg/s and 20 kg/s achieved steady state after 200 days, while the 2 kg/s scenario reached the highest outlet temperature of 19.91 °C but had lowest net energy flow rate of 125.80 kW. It can be concluded that the 2 kg/s case could offer heat recovery options such as greenhouse heating (at surface) or low-grade temperature district heating network systems (sub-surface) where temperatures of 20 °C are favoured, whereas the 20 kg/s could benefit systems that require a higher net energy flow rate (increased from 125.80 kW to 258.38 kW).

Future work should entail carrying out the best-case scenario within the LSSR GDF environment, but with the addition of the anthropogenic heat source term. Careful consideration of mass flow rate will be essential to decipher how much temperature is removed from the GDF to improve its overall safety and mitigate possible THMC processes from the peak temperatures achieved.

ACKNOWLEDGEMENTS

The authors acknowledge assistant from Dr Theo Renaud for initial mesh setup of the CLGS design in the T2Well-EOS1/TOUGH2 software suite. In addition, the authors would also like to thank our colleague from Lawrence Berkeley National Laboratory, Dr Yingqi Zhang, for guidance on the semi-analytical solution in T2Well.

FUNDING

This research is supported by the UK Engineering and Physical Sciences Research Council (EPSRC) [Grant number: EP/R513222/1].

REFERENCES

[1] Bernier F, Lemy F, De Cannière P, Detilleux V. Implications of safety requirements for the treatment of THMC processes in geological disposal systems for radioactive waste. J Rock Mech Geotech Eng 2017;9:428–34. https://doi.org/10.1016/J.JRMGE.2017.04.001.

[2] Thatcher KE, Bond AE, Norris S. Pore pressure response to disposal of heat generating radioactive waste in a low permeability host rock. Int J Rock Mech Min Sci 2020;135:1–11. https://doi.org/10.1016/J.IJRMMS.2020.104456.

[3] NAGRA. Project Opalinus Clay Safety Report Demonstration of disposal feasibility for spent fuel, vitrified high-level waste and long-lived intermediate-level waste. Wettingen: 2002, p. 109.

[4] Zhou X, Sun D, Xu Y. A new thermal analysis model with three heat conduction layers in the nuclear waste repository. Nucl Eng Des 2021;371:110929. https://doi.org/10.1016/J.NUCENGDES.2020.110929.

[5] Chandrasekharam D, Chandrasekhar V. Can Geological Radioactive Waste Disposal Sites Be Used as EGS Sites? Proc. World Geotherm. Congr. 2010, Bali: 2010, p. 1–4.

[6] Doran HR, Renaud T, Brown CS, Kolo I, Falcone G, Sanderson DCW. Radioactive waste as an anthropogenic heat source: shallow and deep geothermal applications. Submitt. to Eur. Geotherm. Congr., Berlin: 2022, p. 7.

[7] IAEA. Status and Trends in Spent Fuel and Radioactive Waste Management . Vienna: 2022.

[8] Energy Pöyry Ltd, Nuclear Wood Ltd. NDA-Nuclear Decommissioning Authority. 2019 UK Radioactive waste inventory. pp 1-70

[9] Holton D, Myers S, Carta G, Hoch A, Dickinson M, Carr N. Application of a novel approach to assess the thermal evolution processes associated with the disposal of high-heat-generating waste in a geological disposal facility. Eng Geol 2016;211:102–19. https://doi.org/10.1016/j.enggeo.2016.06.010.

[10] RWM. Inventory for geological disposal Main Report. Didcot: 2021.

[11] Doran HR, Renaud T, Kolo I, Brown CS, Falcone G, Sanderson DCW. Harnessing Anthroprogenic Heat from Radioactive Waste in Geological Disposal Facility settings via Closed-Loop Geothermal Systems. Submitt. to World Geotherm. Congr. 2022, Beijing: 2022, p. 1–10.

[12] Loukusa, H. and Nordman, H., Feasibility of KBS-3 spent fuel disposal concept for Norwegian spent fuel. 2020. pp1-45

[13] Itälä, Aku. (2018). Chemical behaviour of bentonite in the near field of the KBS-3V concept.

[14] Sundberg J, Back P-E, Christiansson R, Hökmark H, Ländell M, Wrafter J. Modelling of thermal rock mass properties at the potential sites of a Swedish nuclear waste repository. Int J Rock Mech Min Sci 2009;46:1042–54. https://doi.org/10.1016/j.ijrmms.2009.02.004.

[15] Jackson CP, Holton D, Myers S. Project Ankhiale: Estimating the uplift due to high-heat-generating waste in a Geological Disposal Facility . Warrington: 2016.

[16] RWM. Eastern England subregion 2. Didcot: 2018.

[17] RWM. Initial Evaluation Report: Copeland Area together with the adjacent inshore area . Didcot: 2020.

[18] RWM. Initial Evaluation Report: Allerdale Area together with the adjacent inshore area . Didcot: 2020.

[19] RWM. Initial Evaluation Report: Theddlethorpe Gas Terminal Site and surrounding area within the East Lindsey Area . Didcot: 2021.

[20] Winsloe R, Richter A, Vany J. The Emerging (and Proven) Technologies that Could Finally Make Geothermal Scalable. Proc. World Geotherm. Congr., Reykjavik: 2021, p. 1–11.

[21] Kochkin B, Malkovsky V, Yudintsev S, Petrov V, Ojovan M. Problems and perspectives of borehole disposal of radioactive waste. Prog Nucl Energy 2021;139:103867. https://doi.org/10.1016/J.PNUCENE.2021.103867.

[22] Wang G, Song X, Shi Y, Yang R, Yulong F, Zheng R, et al. Heat extraction analysis of a novel multilateral-well coaxial closed-loop geothermal system. Renew Energy 2021;163:974–86. https://doi.org/10.1016/j.renene.2020.08.121.

[23] Budiono A, Suyitno S, Rosyadi I, Faishal A, Ilyas AX. A Systematic Review of the Design and Heat Transfer Performance of Enhanced Closed-Loop Geothermal Systems. Energies 2022, Vol 15, Page 742 2022;15:742. https://doi.org/10.3390/EN15030742.

[24] Wang G, Song X, Song G, Shi Y, Yu C, Xu F, et al. Analyzes of thermal characteristics of a hydrothermal coaxial closed-loop geothermal system in a horizontal well. Int J Heat Mass Transf 2021;180:121755. https://doi.org/10.1016/j.ijheatmasstransfer.2021.121755.

[25] Van Horn A, Amaya A, Higgins B, Muir J, Scherer J, Pilko R, et al. New Opportunities and Applications for Closed-Loop Geothermal Energy Systems. GRC Trans., 2020, p. 1123–43.

[26] Beckers KF, Rangel-Jurado N, Chandrasekar H, Hawkins AJ, Fulton PM, Tester JW. Techno-Economic Performance of Closed-Loop Geothermal Systems for Heat Production and Electricity Generation. Geothermics 2022;100:102318. https://doi.org/10.1016/j.geothermics.2021.102318.

[27] Beckers KF, Johnston HE. Techno-Economic Performance of Eavor-Loop 2.0. 47th Work. Geotherm. Reserv. Eng. Stanford Univ., Stanford: 2022, p. 1-14.

[28] Song X, Shi Y, Li G, Shen Z, Hu X, Lyu Z, et al. Numerical analysis of the heat production performance of a closed loop geothermal system. Renew Energy 2018;120:365–78. https://doi.org/10.1016/J.RENENE.2017.12.065.

[29] Oldenburg C, Pan L, Muir M, Oldenburg CM, Muir MP, Eastman AD, et al. Numerical Simulation of Critical Factors Controlling Heat Extraction from Geothermal Systems Using a Closed-Loop Heat Exchange Method. 41st Work. Geotherm. Reserv. Eng., Stanford: Lawrence Berkeley National Laboratory; 2019, p. 1–8.

[30] Yuan W, Chen Z, Grasby SE, Little E. Closed-loop geothermal energy recovery from deep high enthalpy systems. Renew Energy 2021;177:976–91. https://doi.org/10.1016/J.RENENE.2021.06.028.

[31] Van Oort E, Chen D, Ashok P, Fallah A. Constructing Deep Closed-Loop Geothermal Wells for Globally Scalable Energy Production by Leveraging Oil and Gas ERD and HPHT Well Construction Expertise. Day 2 Tue, March 09, 2021, SPE; 2021, p. 1–38. https://doi.org/10.2118/204097-MS.

[32] Sun F, Yao Y, Li G, Li X. Geothermal energy development by circulating CO2 in a U-shaped closed loop geothermal system. Energy Convers Manag 2018;174:971–82. https://doi.org/10.1016/J.ENCONMAN.2018.08.094.

[33] Tahir MU. Radioactive waste management: Geological disposal facilities (GDF's) and deep boreholes disposal (DBD) opportunities for heat recovery. University of Glasgow, 2022.

[34] Pan L, Oldenburg CM. T2Well—An integrated wellbore–reservoir simulator. Comput Geosci 2014;65:46–55. https://doi.org/10.1016/J.CAGEO.2013.06.005.

[35] Pan L, Oldenburg CM, Wu Y-S, Pruess K. T2Well/ECO2N Version 1.0: Multiphase and Non-Isothermal Model for Coupled Wellbore-Reservoir Flow of Carbon Dioxide and Variable Salinity Water. Berkeley: 2011.

[36] Pruess K, Oldenburg C, Moridis G. TOUGH2 User's Guide, Version 2.1. Berkeley : 2012.

[37] Zhang Y, Pan L, Pruess K, Finsterle S. A time-convolution approach for modeling heat exchange between a wellbore and surrounding formation. Geothermics 2011;40:261–6. https://doi.org/10.1016/J.GEOTHERMICS.2011.08.003.

[38] Doran HR, Renaud T, Falcone G, Pan L, Verdin PG. Modelling an unconventional closed-loop deep borehole heat exchanger (DBHE): sensitivity analysis on the Newberry volcanic setting. Geotherm Energy 2021;9:1–24. https://doi.org/10.1186/S40517-021-00185-0/FIGURES/11.

[39] Renaud T, Pan L, Doran H, Falcone G, Verdin PG. Numerical Analysis of Enhanced Conductive Deep Borehole Heat Exchangers. Sustain 2021;13:1–21. https://doi.org/10.3390/SU13126918.

[40] Busby J. Geothermal Prospects in the United Kingdom. Proc. World Geotherm. Congr., Bali: 2010, p. 25–9.

[41] Parkes D, Busby J, Kemp SJ, Petitclerc E, Mounteney I. The thermal properties of the Mercia Mudstone Group. Q J Eng Geol Hydrogeol 2020:1–10. https://doi.org/10.1144/qjegh2020-098.

[42] Ghavidel A, Gracie R, Dusseault MB. Design parameters impacting electricity generation from horizontal multilateral closed-loop geothermal systems in Hot Dry Rock. Geothermics 2022; 105:1–12.

[43] Esmaeilpour M, Korzani MG, Kohl T. Impact of thermosiphoning on long-term behavior of closed-loop deep geothermal systems for sustainable energy exploitation. Renew Energy 2022; 194:1247–60.

[44] Goldammer, T., 2019. Greenhouse Management - A Guide to Operations and Technology. U.S.A: Apex Publishers.

[45] Lund, H., Østergaard, P.A., Nielsen, T.B., Werner, S., Thorsen, J.E., Gudmundsson, O., Arabkoohsar, A., Mathiesen, B.V., 2021. Perspectives on fourth and fifth generation district heating. Energy 227, 120520